



## Probing hydrogen bonds in the antibody-bound HIV-1 gp120 V3 loop by solid state NMR REDOR measurements

John J. Balbach<sup>a</sup>, Jun Yang<sup>b</sup>, David P. Weliky<sup>b</sup>, Peter J. Steinbach<sup>c</sup>, Vitali Tugarinov<sup>d</sup>, Jacob Anglister<sup>d</sup> & Robert Tycko<sup>a,\*</sup>

<sup>a</sup>Laboratory of Chemical Physics, National Institute of Diabetes and Digestive and Kidney Diseases, National Institutes of Health, Building 5, Room 112, Bethesda, MD 20892-0520, U.S.A.

<sup>b</sup>Department of Chemistry, Michigan State University, East Lansing, MI 48824, U.S.A.

<sup>c</sup>Center for Molecular Modeling, Center for Information Technology, National Institutes of Health, Bethesda, MD 20892-5626, U.S.A.

<sup>d</sup>Department of Structural Biology, Weizmann Institute of Science, Rehovoth, 76100, Israel

Received 8 November 1999; Accepted 17 February 2000

**Key words:** HIV-1, peptide/antibody complex, solid state NMR, V3 loop

### Abstract

We describe solid state NMR measurements on frozen solutions of the complex of the 24-residue HIV-1 gp120 V3 loop peptide RP135 with the Fab fragment of the anti-gp120 antibody 0.5 $\beta$ , using rotational echo double resonance (REDOR). In order to probe possible hydrogen bonding between arginine side chains and glycine backbone carbonyls in the region of the conserved Gly-Pro-Gly-Arg (GPGR) motif of the V3 loop, RP135 samples were prepared with <sup>15</sup>N labels at the  $\eta$  nitrogen positions of arginine side chains and <sup>13</sup>C labels at glycine carbonyl positions and <sup>13</sup>C-detected <sup>13</sup>C-<sup>15</sup>N REDOR measurements were performed on peptide/antibody complexes of these labeled samples. Such hydrogen bonding was previously observed in a crystal structure of the V3 loop peptide/antibody complex RP142/59.1 [Ghiara et al. (1994) *Science*, **264**, 82–85], but is shown by the REDOR measurements to be absent in the RP135/0.5 $\beta$  complex. These results confirm the antibody-dependent conformational differences in the GPGR motif suggested by previously reported solid state NMR measurements of  $\phi$  and  $\Psi$  backbone dihedral angles in the RP135/0.5 $\beta$  complex. In addition, we describe REDOR measurements on the helical synthetic peptide MB(i+4)EK in frozen solution that establish our ability to detect <sup>13</sup>C-<sup>15</sup>N dipole–dipole couplings in the distance range appropriate to these hydrogen bonding studies. We also report the results of molecular modeling calculations on the central portion RP135, using a combination of the solid state NMR restraints of Weliky et al. [*Nat. Struct. Biol.*, **6**, 141–145, 1999] and the liquid state NMR restraints of Tugarinov et al. (*Nat. Struct. Biol.*, **6**, 331–335, 1999). The dynamics calculations demonstrate the mutual compatibility of the two sets of experimental structural restraints and reduce ambiguities in the solid state NMR restraints that result from symmetry and signal-to-noise considerations.

### Introduction

The envelope glycoprotein gp120 is an essential part of the molecular machinery that enables the HIV-1 virus to infect host cells. gp120 binds to CD4 receptors and to secondary chemokine receptors such

as CXCR4 or CCR5 as part of the membrane fusion process whereby viral RNA enters the host (Choe et al., 1996; Cocchi et al., 1996; Trkola et al., 1996; Wu et al., 1996, 1997; Bazan et al., 1998; Dragic et al., 1998; Rizzuto et al., 1998; Berger et al., 1999). The third hypervariable, or V3, loop of gp120 is of particular interest because it is a major immunogenic site of HIV-1 (Matsushita et al., 1988; Javaherian et al., 1989, 1990; Putney et al., 1991; Kliks et al., 1993;

\*To whom correspondence should be addressed. E-mail: tycko@helix.nih.gov

White-Scharf et al., 1993), because deletion of the V3 loop renders the virus uninfected (Freed et al., 1991), and because the amino acid sequence of the V3 loop determines the type of host cell that a particular strain of HIV-1 can infect (Shioda et al., 1992; Cocchi et al., 1996; Berger et al., 1999) through interaction of the V3 loop with chemokine receptors. Although a crystal structure of a ternary protein complex that includes the core of gp120 has been reported (Kwong et al., 1998; Wyatt et al., 1998), the V3 loop was deleted from the gp120 construct in this structure in order to promote crystallization.

Experimental structural information about the V3 loop has been provided by liquid state NMR studies of free V3 peptides (Chandrasekhar et al., 1991; Gupta et al., 1993; Zvi et al., 1995; Campbell et al., 1996; Huang et al., 1996; Vranken et al., 1996; Vu et al., 1996, 1999; Ghiara et al., 1997; Jelinek et al., 1997; Sarma et al., 1997), crystal structures of complexes of V3 peptides with Fab fragments of antibodies raised against V3 peptides (Stura et al., 1992; Rini et al., 1993; Ghiara et al., 1994, 1997; Stanfield et al., 1999), liquid state (Tsang et al., 1997; Zvi et al., 1997; Zvi and Anglister, 1998) and solid state (Weliky et al., 1999) NMR studies of complexes of V3 peptides with Fab fragments of an anti-gp120 antibody, and liquid state NMR studies of the complex of a V3 peptide with Fv fragments of an anti-gp120 antibody (Tugarinov et al., 1999). These structural studies have focussed primarily on the conformation of the V3 loop in the region of a highly conserved Gly-Pro-Gly-Arg (GPGR, residues 319 through 322 in the following discussion) motif, which is included in or close to the epitope of a number of neutralizing antibodies directed against HIV-1 (Matsushita et al., 1988; Javaherian et al., 1989, 1990; Larosa et al., 1990a,b; Stura et al., 1992; Rini et al., 1993; White-Scharf et al., 1993; Ghiara et al., 1994, 1997; Tsang et al., 1997; Zvi et al., 1997; Zvi and Anglister, 1998). Theoretical studies had predicted a type II  $\beta$ -turn conformation for the GPGR motif (Larosa et al., 1990a; Hansen et al., 1996). This prediction was consistent with NMR studies of free V3 peptides, which generally show a fractional population of type I and/or type II turns in the GPGR motif (Chandrasekhar et al., 1991; Gupta et al., 1993; Zvi et al., 1995; Campbell et al., 1996; Huang et al., 1996; Vranken et al., 1996; Vu et al., 1996, 1999; Ghiara et al., 1997; Jelinek et al., 1997; Sarma et al., 1997). Crystal structures of the V3 peptides RP142 and MP1, which derive from the MN strain of HIV-1, bound respectively to Fab fragments of the monoclonal an-

tibodies 59.1 and 50.1, revealed a more complex turn structure (Ghiara et al., 1994; Stanfield et al., 1999). This turn structure was described as a type II  $\beta$ -turn followed by a fused type III/type I turn (Ghiara et al., 1994). Both 59.1 and 50.1 were raised against the 40-residue, disulfide linked peptide RP70 that represents the entire V3 loop of gp120 of the MN strain. A recent solid state NMR study of the complex of the 24-residue V3 peptide RP135, which derives from the IIIB strain of HIV-1, with Fab fragments of the monoclonal antibody 0.5 $\beta$  revealed that the GPGR conformation in the RP135/0.5 $\beta$  complex is both different from that in the RP142/59.1 and MP1/50.1 complexes and inconsistent with the predicted type II  $\beta$ -turn (Weliky et al., 1999). 0.5 $\beta$  was raised against intact gp120 of HIV-1 strain IIIB. This solid state NMR study, which involved two-dimensional magic angle spinning (2D MAS) NMR exchange measurements (Tycko et al., 1996; Weliky and Tycko, 1996) and constant-time double-quantum-filtered dipolar recoupling (CTDQFD) measurements (Bennett et al., 1998b) on frozen solutions of a series of samples in which the antibody-bound peptide was doubly  $^{13}\text{C}$ -labeled at specific positions, placed strong constraints on the dihedral angles  $\phi$  and  $\psi$  that define the peptide backbone conformation in the GPGR motif. Symmetry considerations and signal-to-noise limitations prevented the determination of a unique GPGR backbone conformation from the solid state NMR data (specifically, the  $\phi$  and  $\psi$  angles for Gly321, the second glycine in GPGR, were not determined uniquely). Instead, four possible GPGR conformations were found to be consistent with the data (Weliky et al., 1999). Although a unique conformation was not determined, the solid state NMR measurements, together with the fact that monoclonal antibodies 0.5 $\beta$  and 59.1 both neutralize HIV-1 strain IIIB (Matsushita et al., 1988; White-Scharf et al., 1993), suggested that the GPGR conformation in gp120 is heterogeneous in the unbound form or dependent on the specific antibody in the bound form. The conformational variability revealed in the solid state NMR study also raised the possibility that the conserved nature of the GPGR motif may be a consequence of structural constraints that pertain to the interaction of the V3 loop with chemokine receptors, rather than structural constraints that are present in unbound gp120.

Crystal structures of V3 peptides with Fab fragments of the neutralizing monoclonal antibody 58.2, which was also raised against RP70, have recently been reported in which the GPGR motif adopts a type

I, rather than type II,  $\beta$ -turn (Stanfield et al., 1999). These crystal structures support the notion that the GPGR conformation may be heterogeneous or dependent on complexation with other proteins. Most recently, liquid state NMR measurements have been carried out on the complex of the V3 peptide P1053, which consists of the central 18 residues of RP135, with Fv fragments of 0.5 $\beta$  (Tugarinov et al., 1999). These measurements reveal the existence of a *cis* peptide bond between Gly319 and Pro320 in the GPGR motif, and an overall conformation of the bound peptide described as a  $\beta$ -hairpin with a central type VI  $\beta$ -turn. Both *cis* and *trans* conformations for Pro320 had been shown to be consistent with the solid state NMR data (Weliky et al., 1999). The liquid state NMR data demonstrate that the  $\beta$ -turn in the P1053/0.5 $\beta$  Fv complex is in fact formed by the RGPG sequence (residues Arg318 through Gly321), rather than the GPGR sequence. Residues Gln317 and Arg318 of the V3 loop in gp120 of strain IIIB are absent in gp120 of strain MN, and are therefore absent in the crystal structures (Ghiara et al., 1994; Stanfield et al., 1999). Pro320 is in a *trans* conformation in the crystal structures (Ghiara et al., 1994; Stanfield et al., 1999).

In this paper, we report additional solid state NMR measurements on frozen solutions of the RP135/0.5 $\beta$  Fab complex. These measurements are intended to establish further the qualitative difference between GPGR conformations in the RP135/0.5 $\beta$  and RP142/59.1 complexes. In the crystal structure of the RP142/59.1 Fab complex, the type II  $\beta$ -turn conformation depends on the presence of a hydrogen bond between the  $\epsilon$  nitrogen of the Arg322 side chain and the backbone carbonyl oxygen Gly319 in GPGR (i.e., an *i*-to-*i*+3-side chain hydrogen bond). We report measurements of  $^{13}\text{C}$ - $^{15}\text{N}$  dipole-dipole couplings, using the REDOR technique (Gullion and Schaefer, 1989, 1991; Pan et al., 1990; Garbow and Gullion, 1991; Anderson et al., 1995), that demonstrate the absence of this hydrogen bond in the RP135/0.5 $\beta$  Fab complex. We also demonstrate the absence of similar hydrogen bonding between the side chain of Arg318 and the backbone carbonyl oxygen of Gly321 (i.e., an *i*-side chain-to-*i*+3 hydrogen bond). As a control, we report REDOR measurements on a frozen solution of the helical synthetic peptide MB(i+4)EK (Marqusee and Baldwin, 1987; Marqusee et al., 1989; Long and Tycko, 1998) that confirm our ability to detect  $^{13}\text{C}$ - $^{15}\text{N}$  dipole-dipole couplings in the distance range relevant to the putative hydrogen bonds. Finally, we report the results of molecular modeling calculations in which

structures of the GPGR region of RP135 are derived from a combination of the reported solid state (Weliky et al., 1999) and liquid state (Tugarinov et al., 1999) NMR restraints. The molecular modeling studies demonstrate the mutual compatibility of the two sets of NMR restraints and reduce the ambiguity in the solid state NMR restraints.

The Appendix contains a theoretical treatment of  $^{13}\text{C}$ - $^{15}\text{N}$  REDOR measurements in the presence of  $^{15}\text{N}$ - $^{15}\text{N}$  dipole-dipole couplings. The theoretical results validate our analysis of the RP135/0.5 $\beta$  Fab REDOR data.

## Materials and methods

### Sample preparation

RP135 and MB(i+4)EK peptides were synthesized using solid phase methods on Perkin-Elmer/Applied Biosystems Model 433A and 431A automated synthesizers. The amino acid sequence of RP135 is NNTRK-SIRIQRGPGRAFVTIGKIG, with the N-terminal asparagine and the C-terminal glycine assigned residue numbers 308 and 331, in accordance with the sequence of full-length gp120 of HIV-1 strain IIIB (Rusche et al., 1988; Javaherian et al., 1989). (For comparison, the sequence of the peptide RP142 in the crystal structure of Ghiara et al. is YNKRKRI-HIGPGRAFYTTKNIIGC.) The amino acid sequence of MB(i+4)EK is Ac-AEAAAKEAAAKEAAAKA-NH<sub>2</sub>, with Ac and NH<sub>2</sub> representing N-terminal acetylation and C-terminal amidation. Isotopically labeled, Fmoc-protected alanine was obtained from Cambridge Isotopes. Isotopically labeled glycine and arginine were obtained from Cambridge Isotopes; the latter was converted to Fmoc-protected arginine as described (Chang et al., 1980; Atherton and Sheppard, 1989). In syntheses of RP135, standard Fmoc synthesis and protocols with HOBt/DCC activation were followed, except that coupling times after the labeled arginine were extended and used excess HOBt to suppress side reactions due to the absence of side chain protection on the labeled arginine. All isoleucine residues were double-coupled. In syntheses of MB(i+4)EK, HBTU activation was used. Peptide resins were cleaved according to standard procedures. Peptides were purified by preparative scale reverse-phase HPLC with a binary water/acetonitrile gradient and 0.1% trifluoroacetic acid, using C18 columns. 0.5 $\beta$  antibody Fab fragments were prepared and purified as described (Zvi et al., 1997; Zvi and Anglister, 1998). Solutions of

the RP135/0.5 $\beta$  Fab complex were prepared by mixing solutions of the peptide and Fab in an approximately equimolar ratio, with 10 mM phosphate buffer at pH 7.0, 0.05% NaN<sub>3</sub>, and 10 mM CuNa<sub>2</sub>EDTA to produce proton spin-lattice relaxation times of roughly 0.5 s in the frozen state. Final RP135/0.5 $\beta$  Fab concentrations were approximately 2 mM. MB(i+4)EK concentrations were approximately 4 mM. Solutions of free RP135 and MB(i+4)EK were prepared in a 1:1 w/w mixture of water and glycerol with 10 mM phosphate buffer at pH 7.0 and 10 mM CuNa<sub>2</sub>EDTA. Solutions were transferred into 6-mm-diameter magic angle spinning (MAS) rotors, with sample volumes of 240  $\mu$ l, and frozen by immersion in N<sub>2(l)</sub>. Frozen samples were loaded into the precooled MAS NMR probe for solid state NMR measurements without thawing.

#### *NMR spectroscopy*

Solid state NMR measurements were carried out on a Varian/Chemagnetics Infinity-400 spectrometer, using a Varian/Chemagnetics triple-resonance probe with a 6 mm MAS assembly. The variable-temperature stack provided by Varian/Chemagnetics was extensively modified to increase the flow rate and thermal isolation of cooling gas to the probe, thereby permitting MAS experiments to be performed at a nominal temperature of  $-140^{\circ}\text{C}$  for many consecutive days with an N<sub>2(l)</sub> consumption rate of approximately 6 l/h. <sup>13</sup>C-detected REDOR measurements of <sup>13</sup>C-<sup>15</sup>N dipole-dipole couplings were carried out with the pulse sequence described by Anderson et al. (1995). Transverse <sup>13</sup>C magnetization was prepared by cross-polarization from protons, using a ramped radio-frequency (rf) field on the <sup>13</sup>C channel during cross-polarization to minimize sensitivity to the Hartmann-Hahn matching condition. As described (Anderson et al., 1995), 180° pulses were applied to <sup>13</sup>C nuclei at all multiples of the MAS rotation period during the REDOR dephasing period, i.e., at all times  $n\tau_R$ , where  $\tau_R$  is the MAS rotation period. The dephased <sup>13</sup>C NMR signal  $S_1$  was measured with application of 180° pulses to <sup>15</sup>N nuclei at all times  $(n+1/2)\tau_R$  during the dephasing period. The unde-phased <sup>13</sup>C NMR signal  $S_0$  was measured without the <sup>15</sup>N pulses. XY-8 phase cycling of the 180° pulses was used on both channels (Gullion et al., 1990; Gullion and Schaefer, 1991; Anderson et al., 1995). In the experiments described below,  $\tau_R = 200 \mu\text{s}$  and 180° pulse lengths were approximately 12  $\mu\text{s}$  for both <sup>13</sup>C and <sup>15</sup>N. Proton decoupling fields during the dephasing period were 85 kHz in amplitude. Decoupling

fields during acquisition of <sup>13</sup>C NMR signals were approximately 70 kHz. Rf pulses were actively synchronized with the square-wave tachometer signal from the Varian/Chemagnetics MAS speed controller. Short-term jitter in this tachometer signal due to noise in the optical spin rate detection system in the probe was reduced to less than 0.5  $\mu\text{s}$  by filtering with a home-built phase-locked loop circuit, based on an MC14046B chip. 180° pulse lengths on the <sup>13</sup>C and <sup>15</sup>N channels were optimized respectively by maximizing  $S_0$  and minimizing  $S_1$  in REDOR measurements on a sample of polycrystalline leucine in which 5% of the molecules were <sup>13</sup>C- and <sup>15</sup>N-labeled at the carboxylate and amine positions. These optimizations were performed at low temperature.

#### *NMR data analysis*

REDOR signal amplitudes  $S_1$  and  $S_0$  were extracted from experimental spectra by integrating carbonyl <sup>13</sup>C peaks corresponding to the centerbands and sidebands of order +1 and  $-1$  and then adding the three integrals from each spectrum. Uncertainties in the measurements were estimated by integrating the spectral intensity over equal frequency ranges in regions of the spectra where no <sup>13</sup>C peaks were present and calculating the root-mean-square integral for many such regions. The theoretical REDOR dephasing curve in Figure 5 was calculated from numerical simulations of the orientationally averaged evolution of the nuclear spin density operator under time-dependent dipole-dipole coupling and rf fields, using a two-spin,  $4 \times 4$  matrix representation of the density operator and spin Hamiltonian. Finite pulse lengths were included in these simulations. Inclusion of realistic <sup>15</sup>N and <sup>13</sup>C chemical shift anisotropies was found to produce effects on the simulated REDOR dephasing curves that were negligible compared with the uncertainties in the experimental signals due to noise in the spectra.

#### *Molecular modeling*

The 18-residue peptide P1053, comprising the segment of RP135 from Arg311 through Gly328, was modeled as follows. Four sets of hybrid distance geometry-simulated annealing calculations (Nilges et al., 1988, 1991; Kuszewski et al., 1992) were performed with the XPLOR program (Brünger, 1992), using restraints derived from both liquid (Tugarinov et al., 1999) and solid state (Weliky et al., 1999) NMR data. The final stage of each calculation was 800 steps of Powell energy minimization during which charged side chains were neutralized and nonbonded interac-

tions were approximated with a distance-dependent dielectric coefficient together with Lennard-Jones and hydrogen bond energies. In all calculations, 192 NOE restraints and restraints on 10  $\phi$  angles derived from liquid state NMR measurements on the P1053/0.5 $\beta$  Fv complex (Tugarinov et al., 1999) were applied. The NOE force constant was 50 kcal/mol  $\text{\AA}^2$ . The dihedral angle force constant was 200 kcal/mol  $\text{deg}^2$ . The solid state NMR restraints on  $\phi$  and  $\Psi$  angles of Pro320, Gly321, and Arg322, derived from 2D MAS exchange (Tycko et al., 1996; Weliky and Tycko, 1996) and CTDQFD (Bennett et al., 1998b) measurements, were represented as flat-bottomed potential functions of  $\phi$  and  $\Psi$  with harmonic walls. The  $(\phi, \Psi)$  angles of Pro320 were restrained to within  $10^\circ$  of  $(-68^\circ, 146^\circ)$  and those of Arg322 were restrained to within  $10^\circ$  of  $(-141^\circ, 76^\circ)$ , corresponding to the best fits to the solid state NMR measurements (minima in  $\chi^2$ ) on the RP135/0.5 $\beta$  Fab complex in frozen solution (Weliky et al., 1999). The four sets of calculations differed only in the  $(\phi, \Psi)$  potential minimum to which Gly321 was restrained (to within  $5^\circ$ ). In the discussion below, we refer to these minima of Gly321 at  $(-62^\circ, 71^\circ)$ ,  $(62^\circ, -71^\circ)$ ,  $(-62^\circ, 151^\circ)$ , and  $(62^\circ, -151^\circ)$  as min1, min2, min3, and min4, respectively. In each set of calculations, 50 structures were generated for analysis. As previously discussed (Tycko et al., 1996; Weliky and Tycko, 1996; Weliky et al., 1999), the multiple minima for Gly321 arise from experimental signal-to-noise limitations and from the fact that the solid state NMR data are invariant to the substitution  $\phi, \Psi \rightarrow -\phi, -\Psi$ . For glycine residues in particular, positive values of  $\phi$  must be considered.

## Results

### REDOR measurements on the RP135/0.5 $\beta$ complex

Solid state NMR measurements were performed on frozen solutions of two RP135/0.5 $\beta$  Fab complex samples. In sample I, the peptide was labeled with  $^{13}\text{C}$  at the carbonyl position of Gly319 (i.e., the first glycine in the central GPGR motif) and  $^{15}\text{N}$  at both  $\eta$  nitrogen positions of Arg322. This labeling scheme was chosen to permit a test for the presence of hydrogen bonding between the Arg322 side chain and the Gly319 carbonyl as observed in the RP142/59.1 Fab crystal structure (Ghiara et al., 1994; Stanfield et al., 1999). (Although the  $\epsilon$  nitrogen participates directly in the hydrogen bond in the RP142/59.1 Fab complex, this site was not labeled in our experiments because  $^{15}\text{N}_\epsilon$ -Arg

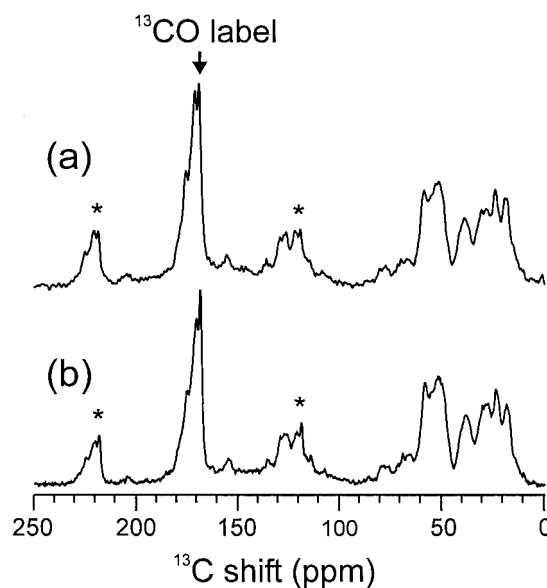


Figure 1.  $^{13}\text{C}$  NMR spectra of frozen solutions of the RP135/0.5 $\beta$  Fab complex in which the RP135 peptide is labeled with  $^{13}\text{C}$  at the carbonyl carbon of Gly319 and  $^{15}\text{N}$  at both  $\eta$  nitrogens of Arg322 (sample I, part a) and with  $^{13}\text{C}$  at the carbonyl carbon of Gly321 and  $^{15}\text{N}$  at both  $\eta$  nitrogens of Arg318 (sample II, part b). The  $^{13}\text{C}$  carrier frequency is 100.8 MHz. Spectra are acquired with cross-polarization, proton decoupling, and magic angle spinning at 5.0 kHz. The nominal sample temperature is  $-140^\circ\text{C}$ . Spectra result from 7200 scans (a) and 6345 scans (b). The sharp peak at 169 ppm arises from the carbonyl  $^{13}\text{C}$  label in both spectra. Other signals are from natural-abundance  $^{13}\text{C}$ . Asterisks indicate spinning sidebands.

was not available from commercial sources.) In the crystal structure, the internuclear distances between the Gly319 carbonyl and the Arg322  $\eta$  nitrogens are 4.24  $\text{\AA}$  and 5.88  $\text{\AA}$ . As demonstrated below by measurements on the MB(i+4)EK peptide,  $^{13}\text{C}$ - $^{15}\text{N}$  distances in this range, particularly a 4.24  $\text{\AA}$  distance, are accessible by REDOR measurements, which is a well-established method for detecting and measuring heteronuclear dipole-dipole couplings in solid state MAS NMR (Gullion and Schaefer, 1989, 1991; Pan et al., 1990; Garbow and Gullion, 1991; Anderson et al., 1995). In sample II, the RP135 peptide was labeled with  $^{13}\text{C}$  at the carbonyl position of Gly321 and  $^{15}\text{N}$  at both  $\eta$  nitrogen positions of Arg318. This labeling scheme permits a test for the presence of hydrogen bonding between the Arg318 side chain and the Gly321 carbonyl. Gln317 and Arg318 of RP135 are absent from RP142, the amino acid sequence of which derives from gp120 of HIV-1 strain MN, so this hydrogen bond was not possible in the RP142/59.1 complex. REDOR measurements on sample II were

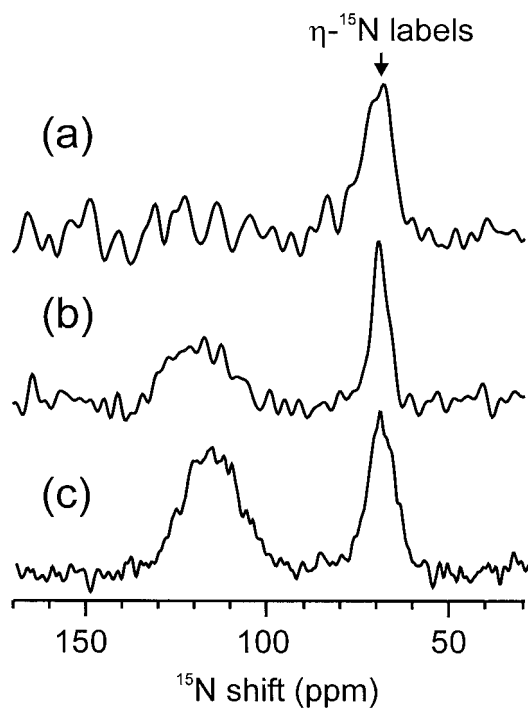


Figure 2.  $^{15}\text{N}$  NMR spectra of a frozen solution of RP135 in glycerol/water with  $^{13}\text{C}$  at the carbonyl carbon of Gly319 and  $^{15}\text{N}$  at both  $\eta$  nitrogens of Arg322 (a) and of aqueous frozen solutions of RP135/0.5 $\beta$  Fab samples I and II (b and c, respectively). The  $^{15}\text{N}$  carrier frequency is 40.6 MHz. Spectra are acquired with cross-polarization, proton decoupling, and magic angle spinning at 5.0 kHz. The nominal sample temperature is  $-140^\circ\text{C}$ . Spectra result from 200 000 scans (a), 8760 scans (b), and 6000 scans (c). Signals at 70 ppm arise from the  $^{15}\text{N}$  labels. Signals near 115 ppm arise primarily from natural-abundance  $^{15}\text{N}$  of the Fab.

motivated by the fact that an Arg318-Gly321 hydrogen bond is possible for some, but not all, GPCR backbone conformations that are consistent with our earlier solid state NMR measurements on the RP135/0.5 $\beta$  Fab complex (Weliky et al., 1999).

Figure 1 shows one-dimensional  $^{13}\text{C}$  NMR spectra of frozen solutions of sample I (Figure 1a) and sample II (Figure 1b), obtained with cross-polarization, MAS at 5.0 kHz, and proton decoupling. The  $^{13}\text{C}$  carrier frequency is 100.8 MHz. Most of the signal intensity arises from natural-abundance  $^{13}\text{C}$  nuclei, due to the approximately 50 kDa molecular weight of the complex. The single  $^{13}\text{C}$  label at glycine carbonyls of RP135 contributes a sharp line at 169 ppm in both spectra. As shown previously (Weliky et al., 1999), observation of this chemical shift and linewidths of 1.5–2.0 ppm for the glycine carbonyls indicate that the peptide is bound and well structured in the frozen solutions.

Figure 2 shows one-dimensional  $^{15}\text{N}$  NMR spectra of frozen solutions of free RP135 labeled at the Gly319 carbonyl and Arg322  $\eta$  nitrogens (Figure 2a), sample I (Figure 2b), and sample II (Figure 2c), obtained with cross-polarization, MAS at 5.0 kHz, and proton decoupling. The  $^{15}\text{N}$  carrier frequency is 40.6 MHz. In all three spectra, the  $^{15}\text{N}$  labels contribute a single peak at 70 ppm. The decrease in linewidth from 9.4 ppm in Figure 2a to 5.3 ppm in Figure 2b is further evidence that the peptide remains bound and structured in frozen solutions of the complex. The fact that the  $\eta$  nitrogen peak in Figure 2c is broader than that in Figure 2b may indicate that the two  $\eta$  nitrogens of Arg318 have a larger chemical shift difference than those of Arg322 in the RP135/0.5 $\beta$  Fab complex, or that the Arg318 side chain is disordered in the complex. The broad peak at 115 ppm in Figures 2b and 2c arises primarily from natural-abundance amide  $^{15}\text{N}$  nuclei. The ratio of natural-abundance amide to labeled  $\eta$  nitrogen signal areas is 1.2:1.0 in Figure 2b and 1.5:1.0 in Figure 2c. For a 1:1 complex, the expected ratio would be approximately 0.9:1.0. This suggests that samples I and II contain an excess of antibody Fab.

In the REDOR measurements on the RP135/0.5 $\beta$  Fab complex,  $^{13}\text{C}$  NMR spectra were obtained with ( $S_1$ ) and without ( $S_0$ ) application of a train of rotor-synchronized  $180^\circ$  pulses at the  $^{15}\text{N}$  NMR frequency during the REDOR dephasing period (Gullion and Schaefer, 1989, 1991; Pan et al., 1990; Garbow and Gullion, 1991; Anderson et al., 1995). Figure 3 shows REDOR sum and difference spectra for sample I (Figure 3a) and sample II (Figure 3b), where the sum spectra are  $S_0 + S_1$  and the difference spectra are  $S_0 - S_1$ . These spectra were obtained with a dephasing period of 61.2 ms, i.e.,  $306\tau_R$  with  $\tau_R = 200 \mu\text{s}$ . For a single  $^{13}\text{C}$ - $^{15}\text{N}$  pair with an internuclear distance of 4.24 Å,  $(S_0 - S_1)/(S_0 + S_1)$  would ideally be 0.85 with a dephasing period of 61.2 ms. The ratio of natural-abundance carbonyl  $^{13}\text{C}$  signal to labeled carbonyl  $^{13}\text{C}$  signal in  $S_0$  is expected to be approximately 6:1. Assuming that only the labeled carbonyl signal is dephased by  $^{13}\text{C}$ - $^{15}\text{N}$  couplings in  $S_1$ ,  $(S_0 - S_1)/(S_0 + S_1)$  should be approximately 0.07 if a hydrogen bond between a  $^{15}\text{N}$ -labeled arginine side chain and a  $^{13}\text{C}$ -labeled glycine carbonyl, similar to what has been observed in the RP142/59.1 Fab complex (Ghiara et al., 1994), is present in the RP145/0.5 $\beta$  Fab complex. In fact, the experimental  $(S_0 - S_1)/(S_0 + S_1)$  values in Figures 3a and 3b, determined by integrating the spectral intensities in

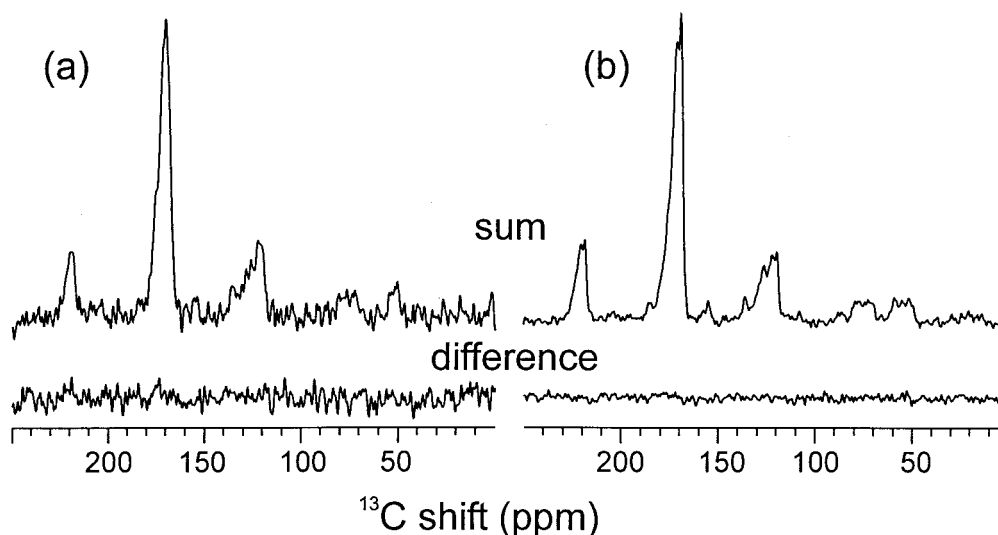


**Figure 3.**  $^{13}\text{C}$ -detected REDOR sum and difference spectra for RP135/0.5 $\beta$  Fab samples I and II (a and b, respectively). The period for  $^{13}\text{C}$ - $^{15}\text{N}$  dephasing is 61.2 ms. The MAS frequency is 5.0 kHz. The total number of scans is 34560 (a) and 38016 (b). The absence of signals above the noise level in the difference spectra indicates the absence of labeled  $^{13}\text{C}$ - $^{15}\text{N}$  pairs with the internuclear distance of approximately 4.2 Å expected if the labeled arginine side chain were hydrogen bonded to the labeled glycine carbonyl. In contrast, hydrogen bonding between the Gly319 carbonyl and the Arg322 side chain has been observed in the crystal structure of a different V3 peptide/antibody complex, namely the RP142/59.1 Fab complex (Ghiara et al., 1994).

the sum and difference spectra over the range from 160 ppm to 185 ppm, are  $0.028 \pm 0.019$  and  $0.0024 \pm 0.0053$ . The stated error limits represent the rms area over a 15 ppm spectral range in regions of the  $^{13}\text{C}$  spectra where there are no NMR signals. In addition, no sharp peaks at 169 ppm are visible above the noise level in either of the difference spectra. We therefore conclude that hydrogen bonds do not exist between the side chain of Arg322 and the carbonyl of Gly319 or between the side chain of Arg318 and the carbonyl of Gly321 in the RP135/0.5 $\beta$  Fab complex.

The analysis above assumes that homonuclear  $^{15}\text{N}$ - $^{15}\text{N}$  dipole-dipole couplings in the doubly labeled arginine side chains do not affect the REDOR measurements. This assumption is justified in the Appendix, which presents a theoretical discussion of the effects of homonuclear couplings.

#### *REDOR measurements on MB(i+4)EK*

The MB(i+4)EK peptide was originally designed by Marqusee and Baldwin (Marqusee and Baldwin, 1987; Marqusee et al., 1989), and called (i+4)EK by them. This 17-residue, polyalanine-based peptide was among the first relatively short synthetic peptides to show high helix contents in aqueous solutions. Solid state NMR measurements and low-temperature CD measurements on glycerol/water so-

lutions of MB(i+4)EK have demonstrated that the helix content near and below the glass transition temperature of the solution (approximately  $-60^\circ\text{C}$ ) is roughly 90% (Long and Tycko, 1998). Solid state NMR measurements on frozen solutions, using the 2D MAS exchange technique (Tycko et al., 1996; Weliky and Tycko, 1996), have provided support for a primarily  $\alpha$ -helical conformation in pure glycerol/water and a heterogeneous helical conformation with substantial  $3_{10}$ -helix content in frozen solutions containing 5.1 M urea (Long and Tycko, 1998). Here we report REDOR measurements on a frozen glycerol/water solution of MB(i+4)EK, with no urea. The peptide is labeled with  $^{15}\text{N}$  at the amide nitrogen of Ala8 and with  $^{13}\text{C}$  at the carbonyl carbons of Ala4 and Ala10. Assuming an  $\alpha$ -helical conformation, the Ala8-Ala4 and Ala8-Ala10  $^{15}\text{N}$ - $^{13}\text{C}$  distances should be approximately 4.2 Å and 5.6 Å, respectively, based on examination of  $\alpha$ -helical segments of proteins with known high-resolution structures. Thus, the distances are about the same as expected for the arginine-glycine hydrogen bonds discussed above.

Figure 4 shows one-dimensional  $^{15}\text{N}$  (Figure 4a) and  $^{13}\text{C}$  (Figure 4b) MAS NMR spectra of a frozen solution of  $^{15}\text{N}$ ,  $^{13}\text{C}_2$ -MB(i+4)EK at a spinning frequency of 5.0 kHz. The two  $^{13}\text{C}$  labels give rise to a single peak at 177 ppm with a 2.0 ppm linewidth,

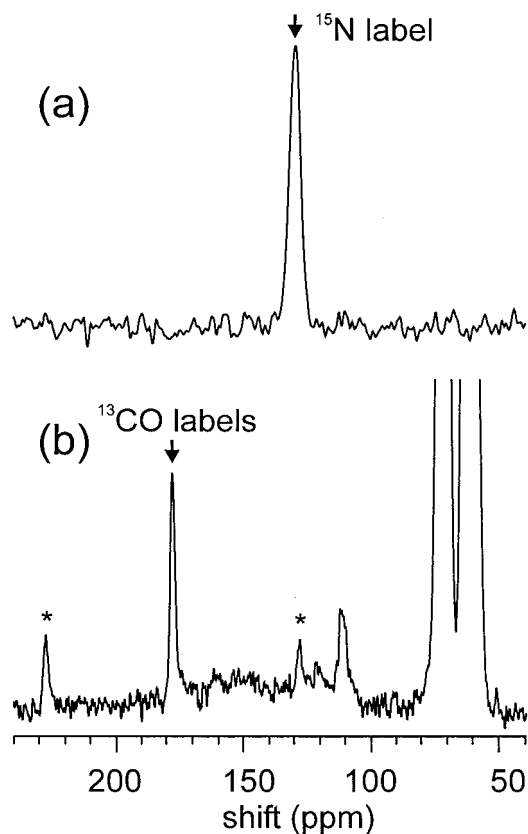


**Figure 4.**  $^{15}\text{N}$  NMR (a) and  $^{13}\text{C}$  NMR (b) spectra of a frozen glycerol/water solution of the synthetic 17-residue peptide MB(i+4)EK, labeled with  $^{15}\text{N}$  at Ala8 and  $^{13}\text{C}$  at the carbonyl carbons of Ala4 and Ala10.  $^{15}\text{N}$  and  $^{13}\text{C}$  carrier frequencies are 40.6 MHz and 100.8 MHz. Spectra are acquired with cross-polarization, proton decoupling, and magic angle spinning at 5.0 kHz. The nominal sample temperature is  $-140^\circ\text{C}$ . Spectra result from 28800 scans (a) and 600 scans (b). Strong signals between 50 and 70 ppm in (b) arise from natural-abundance  $^{13}\text{C}$  of glycerol. Asterisks indicate spinning sidebands.

similar to previously reported spectra of doubly  $^{13}\text{C}$ -labeled MB(i+4)EK. The relatively sharp carbonyl line indicates the predominance of a single type of helical conformation. The  $^{15}\text{N}$  label gives rise to a single line at 130 ppm with a 5.2 ppm linewidth. The broader  $^{15}\text{N}$  line reflects the generally greater sensitivity of amide  $^{15}\text{N}$  chemical shifts to small conformational variations and other structural disorder in the frozen solution.

Figure 5 shows  $^{13}\text{C}$ -detected REDOR  $S_1$  (Figure 5a) and  $S_0$  (Figure 5b) spectra of the frozen  $^{15}\text{N}$ ,  $^{13}\text{C}_2$ -MB(i+4)EK solution with a 38.8 ms REDOR dephasing period. The carbonyl signal intensity in the  $S_1$  spectrum is clearly less than in the  $S_0$  spectrum, demonstrating the REDOR dephasing effect.

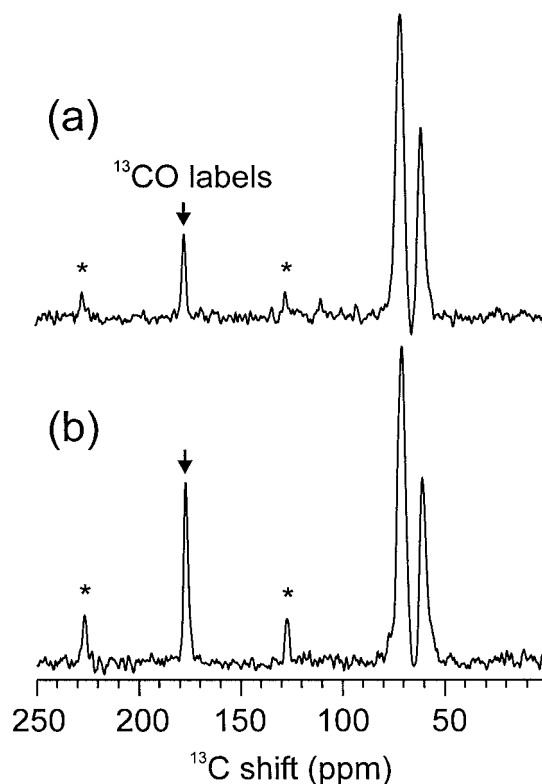


**Figure 5.**  $^{13}\text{C}$  NMR spectra of the triply labeled MB(i+4)EK sample obtained with a REDOR pulse sequence, both with (a) and without (b) the application of  $^{15}\text{N}$  pulses. The period for REDOR dephasing is 38.8 ms. Each spectrum results from 3600 scans. The difference in intensity of the carbonyl signal at 177 ppm is due to  $^{13}\text{C}$ - $^{15}\text{N}$  dephasing when the  $^{15}\text{N}$  pulses are applied. Asterisks indicate spinning sidebands.

Figure 6 shows the dependence of  $S_1/S_0$ , measured by integrating the carbonyl  $^{13}\text{C}$  signal intensities in spectra such as in Figure 5 over the range from 172 ppm to 182 ppm, on the dephasing period. The simulated dephasing curve in Figure 6 was calculated with the assumption that 40% of the carbonyl  $^{13}\text{C}$  nuclei are coupled to a  $^{15}\text{N}$  nucleus at a 4.2 Å distance, 40% are coupled to a  $^{15}\text{N}$  nucleus at a 5.6 Å distance, and 20% are not coupled to  $^{15}\text{N}$  nuclei. The uncoupled  $^{13}\text{C}$  nuclei probably include natural-abundance carbonyl  $^{13}\text{C}$  nuclei that are more than 6 Å away from the  $^{15}\text{N}$  label at Ala8 in helical MB(i+4)EK molecules and  $^{13}\text{C}$  labels in MB(i+4)EK molecules that are non-helical, in roughly equal numbers. The good agreement between the simulated REDOR dephasing curve and the experimental data supports the predominance of the  $\alpha$ -helical conformation in frozen solutions of MB(i+4)EK without denaturant (Long and Tycko, 1998) and establishes our ability to detect  $^{15}\text{N}$ - $^{13}\text{C}$  dipole-dipole couplings

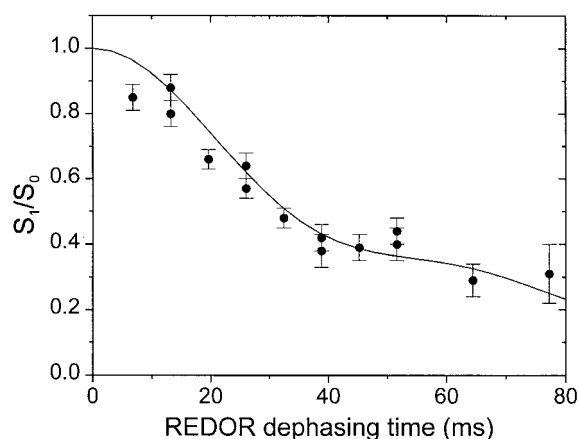


Figure 6. REDOR dephasing curve for the triply labeled MB(i+4)EK sample. The ordinate represents the ratio of carbonyl signal intensities with ( $S_1$ ) and without ( $S_0$ ) the application of  $^{15}\text{N}$  pulses. Filled circles are experimental data points. The solid line is a simulated dephasing curve, assuming that 40% of the carbonyl  $^{13}\text{C}$  nuclei are dephased by dipole-dipole coupling to  $^{15}\text{N}$  with an internuclear distance of 4.2 Å, 40% are dephased by coupling to  $^{15}\text{N}$  with an internuclear distance of 5.6 Å, and 20% are not coupled to  $^{15}\text{N}$ .

in the range that is relevant to the RP135/0.5β Fab measurements described above.

#### Molecular modeling

Structure calculations were performed combining liquid state NOE and J coupling restraints (Tugarinov et al., 1999) and solid state NMR dihedral angle restraints (Weliky et al., 1999) to refine the structure of the antibody-bound V3 loop peptide. Energetic and structural results of the calculations are plotted in Figure 7. Any interatomic distance exceeding the corresponding NOE restraint distance by 0.5 Å or more was considered a violation, as was any dihedral angle more than 5° outside the corresponding restraint range. The fact that the lowest-energy structures for the min1, min2, and min4 calculations exhibit no restraint violations demonstrates the compatibility of the liquid state and solid state NMR measurements. The calculations also suggest that one of the ( $\phi$ ,  $\Psi$ ) pairs for Gly321 that is consistent with the solid state NMR measurements, namely min3, may be ruled out in light of the liquid state NMR measurements. No structures satisfying all NOE and dihedral angle restraints were found in the min3 calculations. In addition, the lowest-energy structures for min3 exhibit strain in bonds, angles, and dihedral angles (Figures 7b and 7c) and consistently higher total potential energies than those of the other three sets of calculations. Figure 8 shows

the lowest-energy structures for the min1, min2, and min4 calculations.

The structures in Figure 8 are dictated by both the liquid state and the solid state NMR restraints. There is little direct overlap between the two sets of constraints. The liquid state data restrain the  $\phi$  angles of residues 313–316, 318, and 323–327, while the solid state data restrain the dihedral angles of residues 320–322. Liquid state NOE restraints on the distances between  $\text{H}_\alpha$  of Pro320 and  $\text{H}_\text{N}$  of Gly321 and between  $\text{H}_\alpha$  of Gly321 and  $\text{H}_\text{N}$  of Arg322 place limits on the possible  $\Psi$  angles of Pro320 and Gly321, respectively, but these limits are not sufficiently restrictive to permit a precise comparison of the liquid state and solid state NMR data. The solid state NMR data place the stronger restraints on the GPGR conformation, while the liquid state NMR data restrain the conformation of the flanking sequences and establish a *cis* conformation for Pro320 through observation of NOEs between the  $\alpha$  protons of Gly319 and Pro320. Since the RP135/0.5β Fab complex remains intact in frozen solution (as supported by the reduction in solid state NMR linewidths upon complexation described above) and since the solid state NMR measurements are carried out on the epitope region of RP135 (i.e., the region that interacts with the antibody binding site), we believe that the peptide conformations probed by the liquid state and solid state NMR measurements are essentially identical. The existence of structural models that are consistent with both sets of measurements supports this belief.

The liquid state NMR measurements of Tugarinov et al. (1999) do not provide direct restraints on the  $\phi$  and  $\Psi$  angles of Gly321. Structural models for P1053 bound to the Fv fragment of 0.5β reported by Tugarinov et al. (1999) have  $\phi$  values for Gly321 (called Gly14 by Tugarinov et al.) in the range from 56° to 99°. While most of these structures have positive  $\Psi$  values for Gly321, two of the reported structures (models 7 and 18 in PDB file 1B03) have  $\Psi$  values of −104° and −145°. These two structures correspond closely to min2 and min4 and are also in best agreement with the restraints on  $\Psi$  of Pro320 and  $\phi$  of Arg322 derived from solid state NMR (Weliky et al., 1999).

#### Discussion and conclusions

The REDOR measurements on the RP135/0.5β Fab complex demonstrate that the hydrogen bond between

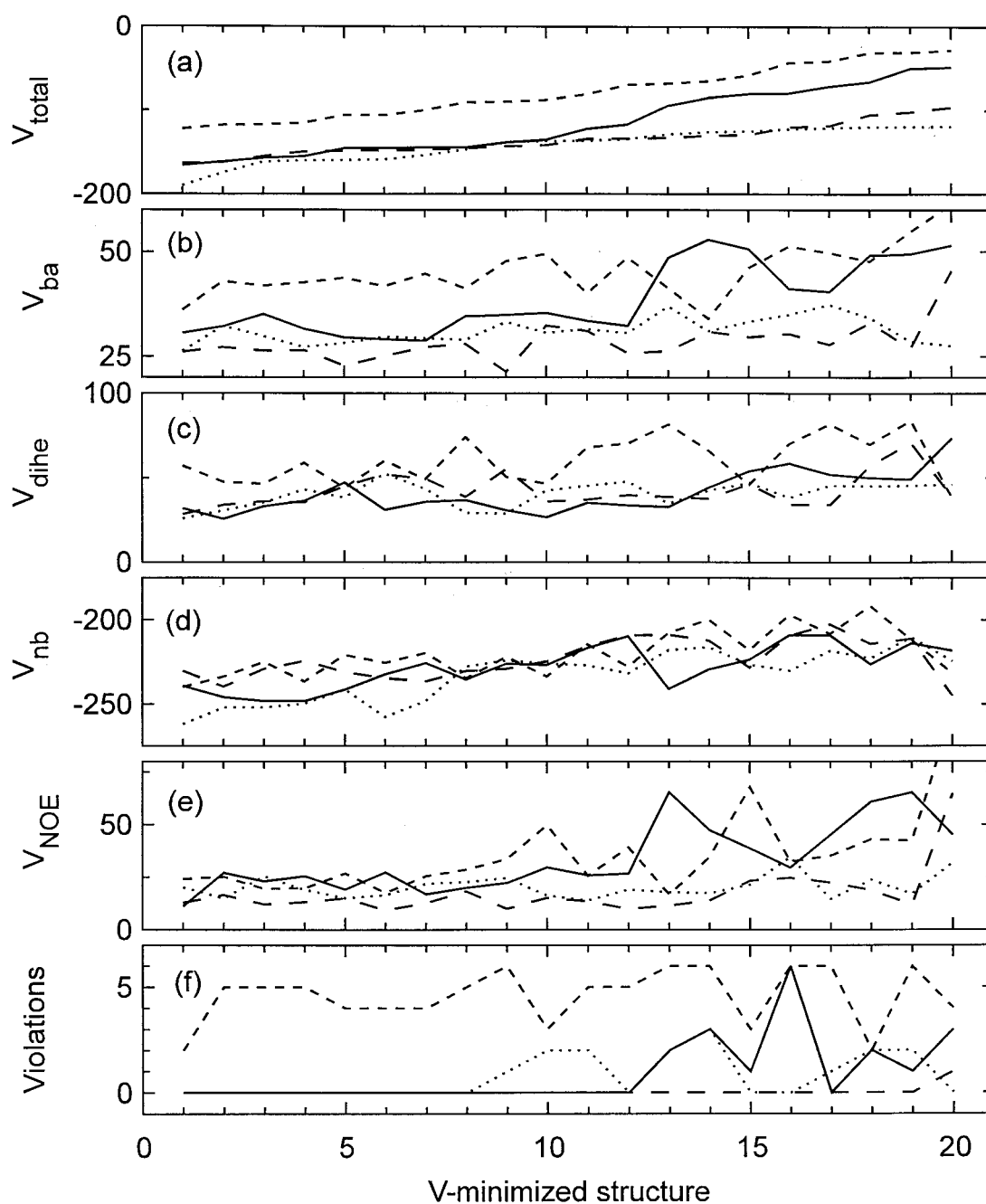
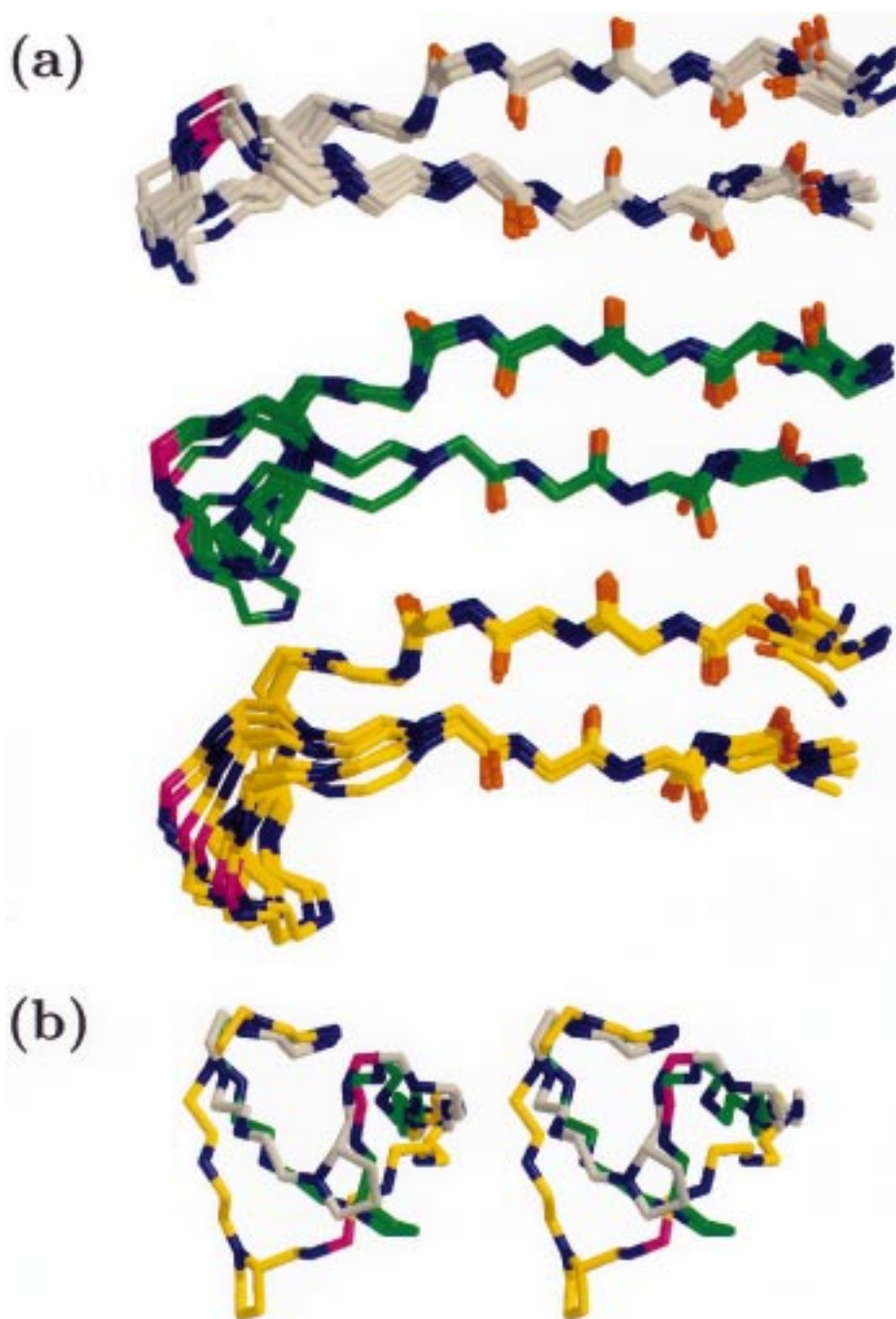


Figure 7. Energies and restraint violations for the 20 structures of lowest energy found for each of the four  $\phi, \psi$  minima for Gly321 consistent with solid state NMR measurements (Weliky et al., 1999): min1 (solid), min2 (dot), min3 (short dash), min4 (long dash). The structures are sorted in order of increasing total potential energy. Plots in each panel indicate total potential energy (a), sum of bond and angle energies (b), sum of dihedral, improper dihedral, and dihedral restraint energies (c), sum of van der Waals, electrostatic, and hydrogen bond energies (d), NOE restraint energy (e), and the sum of NOE violations exceeding a 0.5 Å tolerance and dihedral violations exceeding a 5° tolerance (f).



*Figure 8.* (a) Eight RP135 conformations of lowest energy found for each of three Gly321  $\phi, \psi$  pairs consistent with solid state NMR measurements (Weliky et al., 1999). These structures are derived from a combination of liquid state (Tugarinov et al., 1999) and solid state (Weliky et al., 1999) NMR restraints on the antibody-bound RP135 peptide conformation. All structures were oriented by best-fitting main chain atoms (N, CO, and C $\alpha$ ) of residues 311 to 318 and 324 to 328. The structures were then separated into three sets for display, corresponding to three sets of structure calculations. Only main chain atoms are shown, with nitrogen atoms colored blue, oxygen atoms red, and carbon atoms gray (min1 calculations), green (min2 calculations), or orange (min4 calculations). For clarity, oxygen atoms are not shown for residues 316 to 323. C $\alpha$  of Gly321 is colored purple in each structure. (b) Stereoview of the main chain conformation of residues 316 to 323 for the lowest-energy structures of the min1, min2, and min4 calculations. Structures are oriented as in (a), with the Pro321 ring shown in addition. Graphics were generated using Molscript (Kraulis, 1991) and Raster3d (Merritt and Bacon, 1997).

the Arg322 side chain and the Gly319 carbonyl observed in the RP142/59.1 Fab crystal structure (Ghiara et al., 1994) is absent in the RP135/0.5 $\beta$  Fab complex. In the RP142/59.1 Fab complex, this is the i-to-i+3 hydrogen bond that forms the type II  $\beta$ -turn in the GPGR motif. The absence of this hydrogen bond confirms the earlier solid state NMR (Weliky et al., 1999), liquid state NMR (Tugarinov et al., 1999), and crystallographic (Stanfield et al., 1999) evidence for conformational diversity in the GPGR region in complexes of V3 loop peptides with neutralizing monoclonal antibodies that recognize the V3 loop of HIV-1 gp120. Similar conformational diversity is likely to exist in complexes of these antibodies with full-length gp120 in the context of the intact virus because, although the antibodies in the crystal structures were elicited with peptides rather than full-length gp120 (Rini et al., 1993; Ghiara et al., 1994, 1997; Stanfield et al., 1999), they have nonetheless been shown to neutralize certain HIV-1 strains (Matsushita et al., 1988; White-Scharf et al., 1993). Both 59.1 and 0.5 $\beta$  neutralize HIV-1 strain IIIB, suggesting that the observed conformational differences are not simply strain-dependent. It is likely either that the GPGR region of the V3 loop is conformationally heterogeneous in unbound, full-length gp120 or that complexation with neutralizing antibodies can force conformational changes in the GPGR region. In either case, the possibility remains that the GPGR motif adopts a unique conformation upon interaction with chemokine receptors. The conserved nature of the GPGR motif (Larosa et al., 1990a) may be dictated by structural constraints that come into play in the gp120/chemokine receptor complex.

Recent liquid state NMR and mutagenesis data on the combining site of the P1053/0.5 $\beta$  complex indicate that neither Arg322 nor Arg318 guanido protons of P1053 are involved in intra-peptide hydrogen bonds, in agreement with the solid state NMR data described above. Both of these arginine side chains appear to form intermolecular salt bridges with carboxyl groups in the antibody combining site (V. Tugarinov, personal communication).

The molecular modeling calculations, using both solid state NMR and liquid state NMR restraints, show that three of four classes of GPGR conformations for the RP135/0.5 $\beta$  Fab complex are consistent with both sets of restraints. These correspond to  $\phi, \psi$  angles of approximately  $(-62^\circ, 71^\circ)$ ,  $(62^\circ, -71^\circ)$ , and  $(62^\circ, -151^\circ)$  for Gly321. The symmetry-related values  $(-62^\circ, 151^\circ)$  considered in the earlier solid state NMR work (Weliky et al., 1999) lead to significantly

higher-energy structures when the liquid state NMR restraints are included and can therefore be excluded. In general terms, these calculations demonstrate how precise local structural restraints from solid state NMR measurements can aid in the refinement of global structures determined from liquid state NMR measurements, and how liquid state NMR measurements can remove some of the ambiguities in solid state NMR measurements that are associated with symmetry properties of nuclear spin interaction tensors or signal-to-noise limitations.

## Acknowledgements

This work was supported by a grant to R.T. from the NIH Intramural AIDS Targeted Antiviral Program and by NIH grant GM53329 to J.A. D.P.W. acknowledges support from a Camille and Henry Dreyfus New Faculty Award. We thank S. Matsushita for the hybridoma cell line that produces the 0.5 $\beta$  monoclonal antibody and Y. Ishii for carrying out numerical simulations described in the Appendix.

## References

- Anderson, R.C., Gullion, T., Joers, J.M., Shapiro, M., Villhauer, E.B. and Weber, H.P. (1995) *J. Am. Chem. Soc.*, **117**, 10546–10550.
- Atherton, E. and Sheppard, R.C. (1989) In *Solid Phase Peptide Synthesis*. Practical Approach Series (Rickwood, D. and Hames, B.D., Eds.), IRL Press, New York, NY.
- Bazan, H.A., Alkhatib, G., Broder, C.C. and Berger, E.A. (1998) *J. Virol.*, **72**, 4485–4491.
- Bennett, A.E., Ok, J.H., Griffin, R.G. and Vega, S. (1992) *J. Chem. Phys.*, **96**, 8624–8627.
- Bennett, A.E., Rienstra, C.M., Griffiths, J.M., Zhen, W.G., Lansbury, P.T. and Griffin, R.G. (1998a) *J. Chem. Phys.*, **108**, 9463–9479.
- Bennett, A.E., Weliky, D.P. and Tycko, R. (1998b) *J. Am. Chem. Soc.*, **120**, 4897–4898.
- Berger, E.A., Murphy, P.M. and Farber, J.M. (1999) *Annu. Rev. Immunol.*, **17**, 657–700.
- Brünger, A.T. (1992) *XPLOR. A System for X-ray Crystallography and NMR*, Yale University Press, New Haven, CT.
- Campbell, A.P., Sykes, B.D., Norrby, E., AssaMunt, N. and Dyson, H.J. (1996) *Fold. Des.*, **1**, 157–165.
- Chandrasekhar, K., Profy, A.T. and Dyson, H.J. (1991) *Biochemistry*, **30**, 9187–9194.
- Chang, C.D., Waki, M., Ahmad, M., Meienhofer, J., Lundell, E.O. and Haug, J.D. (1980) *Int. J. Pept. Protein Res.*, **15**, 59–66.
- Choe, H., Farzan, M., Sun, Y., Sullivan, N., Rollins, B., Ponath, P.D., Wu, L.J., Mackay, C.R., LaRosa, G., Newman, W., Gerard, N., Gerard, C. and Sodroski, J. (1996) *Cell*, **85**, 1135–1148.
- Cocchi, F., DeVico, A.L., GarzinoDemo, A., Cara, A., Gallo, R.C. and Lusso, P. (1996) *Nat. Med.*, **2**, 1244–1247.

- Dragic, T., Trkola, A., Lin, S.W., Nagashima, K.A., Kajumo, F., Zhao, L., Olson, W.C., Wu, L.J., Mackay, C.R., Allaway, G.P., Sakmar, T.P., Moore, J.P. and Maddon, P.J. (1998) *J. Virol.*, **72**, 279–285.
- Freed, E.O., Myers, D.J. and Risser, R. (1991) *J. Virol.*, **65**, 190–194.
- Garbow, J.R. and Gullion, T. (1991) *J. Magn. Reson.*, **95**, 442–445.
- Ghiara, J.B., Ferguson, D.C., Satterthwait, A.C., Dyson, H.J. and Wilson, I.A. (1997) *J. Mol. Biol.*, **266**, 31–39.
- Ghiara, J.B., Stura, E.A., Stanfield, R.L., Profy, A.T. and Wilson, I.A. (1994) *Science*, **264**, 82–85.
- Gullion, T., Baker, D.B. and Conradi, M.S. (1990) *J. Magn. Reson.*, **89**, 479–484.
- Gullion, T. and Schaefer, J. (1989) *J. Magn. Reson.*, **81**, 196–200.
- Gullion, T. and Schaefer, J. (1991) *J. Magn. Reson.*, **92**, 439–442.
- Gullion, T. and Vega, S. (1992) *Chem. Phys. Lett.*, **194**, 423–428.
- Gupta, G., Anantharamaiah, G.M., Scott, D.R., Eldridge, J.H. and Myers, G. (1993) *J. Biomol. Struct. Dyn.*, **11**, 345–366.
- Hansen, J.E., Lund, O., Nielsen, J.O., Brunak, S. and Hansen, J.E.S. (1996) *Proteins*, **25**, 1–11.
- Huang, X.L., Smith, M.C., Berzofsky, J.A. and Barchi, J.J. (1996) *FEBS Lett.*, **393**, 280–286.
- Javaherian, K., Langlois, A.J., Larosa, G.J., Profy, A.T., Bolognesi, D.P., Herlihy, W.C., Putney, S.D. and Matthews, T.J. (1990) *Science*, **250**, 1590–1593.
- Javaherian, K., Langlois, A.J., McDanal, C., Ross, K.L., Eckler, L.I., Jellis, C.L., Profy, A.T., Rusche, J.R., Bolognesi, D.P., Putney, S.D. and Matthews, T.J. (1989) *Proc. Natl. Acad. Sci. USA*, **86**, 6768–6772.
- Jelinek, R., Terry, T.D., Gesell, J.J., Malik, P., Perham, R.N. and Opella, S.J. (1997) *J. Mol. Biol.*, **266**, 649–655.
- Kliks, S.C., Shioda, T., Haigwood, N.L. and Levy, J.A. (1993) *Proc. Natl. Acad. Sci. USA*, **90**, 11518–11522.
- Kraulis, P.J. (1991) *J. Appl. Crystallogr.*, **24**, 946–950.
- Kuszewski, J., Nilges, M. and Brünger, A.T. (1992) *J. Biomol. NMR*, **2**, 33–56.
- Kwong, P.D., Wyatt, R., Robinson, J., Sweet, R.W., Sodroski, J. and Hendrickson, W.A. (1998) *Nature*, **393**, 648–659.
- Larosa, G.J., Davide, J.P., Weinhold, K., Waterbury, J.A., Profy, A.T., Lewis, J.A., Langlois, A.J., Dreesman, G.R., Boswell, R.N., Shaddock, P., Holley, L.H., Karplus, M., Bolognesi, D.P., Matthews, T.J., Emini, E.A. and Putney, S.D. (1990a) *Science*, **249**, 932–935.
- Larosa, G.J., Javaherian, K., Profy, A., Rusche, J., Weinhold, K., Langlois, A., Matthews, T., Bolognesi, D., Emini, E., Gallo, R., Putney, S. and Wongstaal, F. (1990b) *Aids Res. Hum. Retrovir.*, **6**, 30–31.
- Long, H.W. and Tycko, R. (1998) *J. Am. Chem. Soc.*, **120**, 7039–7048.
- Marqusee, S. and Baldwin, R.L. (1987) *Proc. Natl. Acad. Sci. USA*, **84**, 8898–8902.
- Marqusee, S., Robbins, V.H. and Baldwin, R.L. (1989) *Proc. Natl. Acad. Sci. USA*, **86**, 5286–5290.
- Matsushita, S., Robertguroff, M., Rusche, J., Koito, A., Hattori, T., Hoshino, H., Javaherian, K., Takatsuki, K. and Putney, S. (1988) *J. Virol.*, **62**, 2107–2114.
- Merritt, E.A. and Bacon, D.J. (1997) *Methods Enzymol.*, **277**, 505–524.
- Nilges, M., Clore, G.M. and Gronenborn, A.M. (1988) *FEBS Lett.*, **229**, 317–324.
- Nilges, M., Kuszewski, J. and Brünger, A.T. (1991) In *Computational Aspects of the Study of Biological Macromolecules by NMR Spectroscopy* (Hoch, J.C., Poulsen, F.M. and Redfield, C., Eds.), Plenum Press, New York, NY.
- Pan, Y., Gullion, T. and Schaefer, J. (1990) *J. Magn. Reson.*, **90**, 330–340.
- Putney, S.D., Javaherian, K.J., Larosa, G.J., Emilio, E.A., Lewis, J.A., Langlois, A.J., Bolognesi, D.P. and Matthews, T.J. (1991) *Aids Res. Hum. Retrovir.*, **7**, 145.
- Rini, J.M., Stanfield, R.L., Stura, E.A., Salinas, P.A., Profy, A.T. and Wilson, I.A. (1993) *Proc. Natl. Acad. Sci. USA*, **90**, 6325–6329.
- Rizzuto, C.D., Wyatt, R., Hernandez-Ramos, N., Sun, Y., Kwong, P.D., Hendrickson, W.A. and Sodroski, J. (1998) *Science*, **280**, 1949–1953.
- Rusche, J.R., Javaherian, K., McDanal, C., Petro, J., Lynn, D.L., Grimaila, R., Langlois, A., Gallo, R.C., Arthur, L.O., Fischinger, P.J., Bolognesi, D.P., Putney, S.D. and Matthews, T.J. (1988) *Proc. Natl. Acad. Sci. USA*, **85**, 3198–3202.
- Sarma, A.V.S., Raju, T.V. and Kunwar, A.C. (1997) *J. Biochem. Biophys. Methods*, **34**, 83–98.
- Shioda, T., Levy, J.A. and Chengmayer, C. (1992) *Proc. Natl. Acad. Sci. USA*, **89**, 9434–9438.
- Stanfield, R.L., Cabezas, E., Satterthwait, A.C., Stura, E.A., Profy, A.T. and Wilson, I.A. (1999) *Struct. Fold. Des.*, **7**, 131–142.
- Stura, E.A., Stanfield, R.L., Fieser, G.G., Silver, S., Roguska, M., Hincapie, L.M., Simmerman, H.K.B., Profy, A.T. and Wilson, I.A. (1992) *Proteins*, **14**, 499–508.
- Trkola, A., Dragic, T., Arthos, J., Binley, J.M., Olson, W.C., Allaway, G.P., ChengMayer, C., Robinson, J., Maddon, P.J. and Moore, J.P. (1996) *Nature*, **384**, 184–187.
- Tsang, P., Mu, X.Y., Wu, G. and Durda, P.J. (1997) *J. Mol. Recogn.*, **10**, 256–261.
- Tugarinov, V., Zvi, A., Levy, R. and Anglister, J. (1999) *Nat. Struct. Biol.*, **6**, 331–335.
- Tycko, R., Weliky, D.P. and Berger, A.E. (1996) *J. Chem. Phys.*, **105**, 7915–7930.
- Vranken, W.F., Budesinsky, M., Martins, J.C., Fant, F., Boulez, K., Gras-Masse, H. and Borremans, F.A.M. (1996) *Eur. J. Biochem.*, **236**, 100–108.
- Vu, H.M., deLorimier, R., Moody, M.A., Haynes, B.F. and Spicer, L.D. (1996) *Biochemistry*, **35**, 5158–5165.
- Vu, H.M., Myers, D., de Lorimier, R., Matthews, T.J., Moody, M.A., Heinly, C., Torres, J.V., Haynes, B.F. and Spicer, L. (1999) *J. Virol.*, **73**, 746–750.
- Weliky, D.P., Bennett, A.E., Zvi, A., Anglister, J., Steinbach, P.J. and Tycko, R. (1999) *Nat. Struct. Biol.*, **6**, 141–145.
- Weliky, D.P. and Tycko, R. (1996) *J. Am. Chem. Soc.*, **118**, 8487–8488.
- White-Scharf, M.E., Potts, B.J., Smith, L.M., Sokolowski, K.A., Rusche, J.R. and Silver, S. (1993) *Virology*, **192**, 197–206.
- Wu, L.J., Gerard, N.P., Wyatt, R., Choe, H., Parolin, C., Ruffing, N., Borsetti, A., Cardoso, A.A., Desjardins, E., Newman, W., Gerard, C. and Sodroski, J. (1996) *Nature*, **384**, 179–183.
- Wu, L.J., LaRosa, G., Kassam, N., Gordon, C.J., Heath, H., Ruffing, N., Chen, H., Humblis, J., Samson, M., Parmentier, M., Moore, J.P. and Mackay, C.R. (1997) *J. Exp. Med.*, **186**, 1373–1381.
- Wyatt, R., Kwong, P.D., Desjardins, E., Sweet, R.W., Robinson, J., Hendrickson, W.A. and Sodroski, J.G. (1998) *Nature*, **393**, 705–711.
- Zvi, A. and Anglister, J. (1998) *Letts. Pept. Sci.*, **5**, 357–364.
- Zvi, A., Feigelson, D.J., Hayek, Y. and Anglister, J. (1997) *Biochemistry*, **36**, 8619–8627.
- Zvi, A., Kustanovich, I., Hayek, Y., Matsushita, S. and Anglister, J. (1995) *FEBS Lett.*, **368**, 267–270.

## Appendix

### *Effects of $^{15}\text{N}$ - $^{15}\text{N}$ coupling on $^{13}\text{C}$ - $^{15}\text{N}$ REDOR measurements*

In this Appendix, we analyze the effects of dipole–dipole coupling between the two  $^{15}\text{N}$ -labeled  $\eta$  nitrogens of arginine on REDOR dephasing of a  $^{13}\text{C}$ -labeled glycine carbonyl carbon. In the putative arginine-glycine hydrogen bond described above, the  $^{13}\text{C}$ - $^{15}\text{N}$  distances are approximately 4.24 Å and 5.88 Å, so that the heteronuclear dipole–dipole couplings differ by a factor of 2.67. The  $^{15}\text{N}$ - $^{15}\text{N}$  distance is approximately 2.38 Å. Thus, the homonuclear  $^{15}\text{N}$ - $^{15}\text{N}$  dipole–dipole coupling exceeds the stronger  $^{13}\text{C}$ - $^{15}\text{N}$  coupling by a factor of roughly 20, in the case of a non-spinning sample. In the REDOR measurements described above, MAS with rotation period  $\tau_{\text{R}} = 200 \mu\text{s}$  is used. Rotor-synchronized  $180^\circ$  pulses are applied to  $^{13}\text{C}$  and  $^{15}\text{N}$  nuclei to recouple the heteronuclear coupling. The  $^{15}\text{N}$  pulses have the potential of recoupling the homonuclear coupling, as occurs in the radio-frequency-driven recoupling (RFDR) technique (Bennett et al., 1992, 1998a,b; Gullion and Vega, 1992). One then wonders whether the  $^{15}\text{N}$ - $^{15}\text{N}$  coupling may interfere with the detection of the  $^{13}\text{C}$ - $^{15}\text{N}$  coupling in a REDOR measurement. To analyze this problem theoretically, consider the following Hamiltonian for a spin system consisting of one  $^{13}\text{C}$  nucleus (spin I) and two  $^{15}\text{N}$  nuclei (spins  $S_1$  and  $S_2$ ) during the REDOR pulse sequence:

$$\begin{aligned} H(t) = & \omega_1(t)I_z + \omega_{S1}(t)S_{z1} + \omega_{S2}(t)S_{z2} \\ & + d_{\text{IS}}(t)I_zS_{z1} + d_{\text{SS}}(t) \\ & \left[ S_{z1}S_{z2} - \frac{1}{4}(S_{1+}S_{2-} + S_{1-}S_{2+}) \right] \end{aligned} \quad (\text{A1})$$

The terms on the right side of Equation A1 represent the chemical shift of spin I, the chemical shift of spin  $S_1$ , the chemical shift of spin  $S_2$ , the heteronuclear dipole–dipole coupling between spins I and  $S_1$ , and the homonuclear dipole–dipole coupling between spins  $S_1$  and  $S_2$ , respectively. For simplicity, coupling between I and  $S_2$  is ignored.  $H(t)$  is taken to be the Hamiltonian in an interaction representation with respect to the pulse sequence applied to the I and S spins. This pulse sequence consists of  $180^\circ$  pulses applied to the I spin at integer multiples of  $\tau_{\text{R}}$  and to the S spins at half-integer multiples of  $\tau_{\text{R}}$ , i.e., at times equal to  $(n + 1/2)\tau_{\text{R}}$ . Pulse durations are assumed to be negligibly short. The chemical shift and coupling coefficients are time-dependent because of MAS and because of the pulse sequence. The period of  $d_{\text{SS}}(t)$

and  $d_{\text{IS}}(t)$  is  $\tau_{\text{R}}$ . The period of  $\omega_1(t)$ ,  $\omega_{S1}(t)$ , and  $\omega_{S2}(t)$  is  $2\tau_{\text{R}}$ , and these chemical shift coefficients average to zero over one period. The net spin evolution over one period of  $H(t)$  is described by the operator  $U(2\tau_{\text{R}})$ , which can be written as:

$$U(2\tau_{\text{R}}) = U_{\text{IS}}(2\tau_{\text{R}})U_{\text{SS}}(2\tau_{\text{R}}) \quad (\text{A2})$$

$$U_{\text{IS}}(t) = \exp \left\{ -i \int_0^t dt' [\omega_{S1}(t')S_{z1} + \omega_{S2}(t')S_{z2} + d_{\text{IS}}(t')I_zS_{z1}] \right\} \quad (\text{A3})$$

$$U_{\text{IS}}(2\tau_{\text{R}}) = \exp(-i\phi_{\text{IS}}I_zS_{z1}) \quad (\text{A4})$$

$$\begin{aligned} U_{\text{SS}}(2\tau_{\text{R}}) = & \bar{T} \exp \left\{ -i \int_0^{2\tau_{\text{R}}} dt d_{\text{SS}}(t) [S_{z1}S_{z2} \right. \\ & \left. - \frac{1}{4}U_{\text{IS}}(t)^{-1}(S_{1+}S_{2-} + S_{1-}S_{2+})U_{\text{IS}}(t)] \right\} \\ & \approx \exp [2i(DS_{1+}S_{2-} + D^{\dagger}S_{1-}S_{2+})\tau_{\text{R}}] \end{aligned} \quad (\text{A5})$$

$$\begin{aligned} D = & \frac{1}{8\tau_{\text{R}}} \int_0^{2\tau_{\text{R}}} dt d_{\text{SS}}(t) \exp \left\{ i \int_0^t dt' [\omega_{S1}(t') \right. \\ & \left. - \omega_{S2}(t') + d_{\text{IS}}(t')I_z] \right\} \end{aligned} \quad (\text{A6})$$

$U_{\text{SS}}(2\tau_{\text{R}})$  is the evolution operator for the homonuclear coupling in an interaction representation with respect to the other terms in  $H(t)$ .  $D$  represents the effective homonuclear coupling strength, recoupled by the S-spin pulse train. In an analysis of the RFDR technique for a two-spin, homonuclear system,  $D$  would be a scalar. Here,  $D$  is an operator on the I spin because the state of the I spin affects the time dependence of the local magnetic field at  $S_1$  and hence affects the extent of RFDR recoupling.

Assuming that transverse magnetization is initially prepared on I and that signals from I are detected, the NMR signal after  $2N$  rotation periods is

$$\begin{aligned}
S(N) &= \text{Tr}_{I, S_1, S_2} \left\{ \mathbf{I}_+ [\mathbf{U}_{IS}(2\tau_R) \mathbf{U}_{SS}(2\tau_R)]^N \right. \\
&\quad \left. \mathbf{I}_x [\mathbf{U}_{SS}(2\tau_R)^{-1} \mathbf{U}_{IS}(2\tau_R)^{-1}]^N \right\} \\
&= \frac{1}{2} \text{Tr}_{S_1, S_2} \left\{ \left[ \exp\left(i \frac{\phi_{IS}}{2} S_{z1}\right) \right. \right. \\
&\quad \left. \left. \exp\left[2i(D_- S_{1+} S_{2-} + D_-^* S_{1-} S_{2+}) \tau_R\right] \right]^N \right. \\
&\quad \times \left[ \exp\left[-2i(D_+ S_{1+} S_{2-} \right. \right. \\
&\quad \left. \left. + D_+^* S_{1-} S_{2+}) \tau_R\right] \exp\left(i \frac{\phi_{IS}}{2} S_{z1}\right) \right]^N \left. \right\} \\
&= \frac{1}{2} \text{Tr}_{S_1, S_2} \left\{ \exp\left(i \frac{N\phi_{IS}}{2} S_{z1}\right) \right. \quad (A7) \\
&\quad \left. \prod_{k=0}^{N-1} \exp\left[2i(D_- e^{-i\phi_{IS}k/2} S_{1+} S_{2-} \right. \right. \\
&\quad \left. \left. + D_-^* e^{i\phi_{IS}k/2} S_{1-} S_{2+}) \tau_R\right] \right. \\
&\quad \times \prod_{k'=0}^{N-1} \exp\left[-2i(D_+ e^{i\phi_{IS}k'/2} S_{1+} S_{2-} \right. \\
&\quad \left. + D_+^* e^{-i\phi_{IS}k'/2} S_{1-} S_{2+}) \tau_R\right] \\
&\quad \left. \exp\left(i \frac{N\phi_{IS}}{2} S_{z1}\right) \right\}
\end{aligned}$$

In Equation A7,  $D_{\pm} = (\pm |D| +)$ . The product over the index  $k$  is evaluated in increasing order. The product over the index  $k'$  is evaluated in decreasing order.

The quantities  $|\phi_{IS}|$  and  $|D_{\pm}\tau_R|$  represent the magnitudes of the REDOR and RFDR recoupling effects, respectively. If  $|D_{\pm}\tau_R| \ll 1$  and  $|\phi_{IS}| \gg |D_{\pm}\tau_R|$ , i.e., if the recoupled heteronuclear coupling is much larger than the recoupled homonuclear coupling, then

$$\begin{aligned}
&\prod_{k=0}^{N-1} \exp\left[2i(D_- e^{-i\phi_{IS}k/2} S_{1+} S_{2-} \right. \\
&\quad \left. + D_-^* e^{i\phi_{IS}k/2} S_{1-} S_{2+}) \tau_R\right] \\
&\approx \exp\left\{2i\left[D_- S_{1+} S_{2-} \left(\sum_{k=0}^{N-1} e^{-i\phi_{IS}k/2}\right) \right. \right. \\
&\quad \left. \left. + D_-^* S_{1-} S_{2+} \left(\sum_{k'=0}^{N-1} e^{i\phi_{IS}k'/2}\right) \tau_R\right] \right\} \quad (A8) \\
&\approx 1
\end{aligned}$$

and similarly for the product involving  $D_+$ . (More rigorously, it may be necessary to break the product over  $k$  into several pieces if  $|ND_{\pm}\tau_R| \sim 1$ .) In this limit, the NMR signal becomes

$$\begin{aligned}
S(N) &= \text{Tr}_{S_1} \left\{ \exp(iN\phi_{IS} S_{z1}) \right\} \\
&= 2 \cos(N\phi_{IS}/2) \quad (A9)
\end{aligned}$$

The signal in Equation A9 is simply the REDOR signal in the absence of the S-spin homonuclear coupling, with  $\pm\phi_{IS}/2$  being the net precession angle of spin I due to coupling to spin  $S_1$  over a period  $2\tau_R$ .

The derivation of Equation A9 depends on the assumption that REDOR recoupling dominates RFDR recoupling. In fact, in the limit of negligibly short  $180^\circ$  pulses, numerical simulations of RFDR recoupling between two  $^{15}\text{N}$  spins with an internuclear distance of 2.38 Å, CSA widths of roughly 1.5 kHz, and  $\tau_R = 200 \mu\text{s}$  indicate a characteristic time for RFDR recoupling on the order of 300 ms. The characteristic time for REDOR recoupling for a 4.2 Å  $^{13}\text{C}$ - $^{15}\text{N}$  distance is on the order of 20 ms, as shown in Figure 6. Thus, we expect the derivation above to apply in this case. Numerical simulations of the REDOR experiment for the full three-spin system (i.e., one carbonyl  $^{13}\text{C}$  and two  $^{15}\text{N}$  nuclei, with one  $^{13}\text{C}$ - $^{15}\text{N}$  distance of 4.2 Å and a  $^{15}\text{N}$ - $^{15}\text{N}$  distance of either 2.4 Å or 1000 Å, with finite  $180^\circ$  pulses, and with  $^{15}\text{N}$  CSA widths up to 4.1 kHz) also indicate that the  $^{15}\text{N}$ - $^{15}\text{N}$  coupling does not affect the  $^{13}\text{C}$ - $^{15}\text{N}$  REDOR dephasing curve significantly.